Journal of Nuclear Materials 443 (2013) 152–160

Contents lists available at SciVerse ScienceDirect

Journal of Nuclear Materials

journal homepage: www.elsevier.com/locate/jnucmat

# Constitutive modeling for the anisotropic uniaxial ratcheting behavior of Zircaloy-4 alloy at room temperature

Hua Li [a], Mingjian Wen [a], Gang Chen [a], Weiwei Yu [b], Xu Chen [a,*]

[a] School of Chemical Engineering and Technology, Tianjin University, Tianjin 300072, China
[b] Suzhou Nuclear Power Institute, Suzhou 240051, China

ARTICLE INFO

*Article history:*
Received 17 December 2012
Accepted 29 June 2013
Available online 9 July 2013

ABSTRACT

A series of monotonic tensile, compressive and uniaxial ratcheting tests are conducted at room temperature on Zircaloy-4 (Zr-4) tubes to investigate the mechanical behaviors under various loading conditions. The experimental results show that the ratcheting strain is sensitive to mean stress, stress amplitude and mean stress direction. It is found that the material features anisotropy both in monotonic tests and uniaxial ratcheting tests with different mean stress directions. The difference of mechanical properties under tensile and compressive loading, especially the yield stress, is believed to contribute to the anisotropic ratcheting behavior of the material. In order to describe the anisotropic nature of the uniaxial ratcheting behavior of Zr-4, an anisotropic Ohno–Wang (OW) constitutive model introducing an initial back stress is developed. The results predicted show reasonable agreement with the experimental data.



## 1. Introduction

Zircaloy-4 (Zr-4) is a zirconium based Zr–Sn alloy, which is used as fuel cladding in Pressurized Water Reactors (PWR) [1]. The fuel cladding is subjected to cyclic loading to plastic deformation due to the power fluctuation during service. Therefore, it is essential to study the cyclic plastic deformation behavior of Zr-4 in order to develop advanced fuel assemblies, and to ensure the integrity of fuel cladding currently employed in operating reactors. A number of low cycle fatigue [2,3] and some high cycle fatigue [4] tests for the material have been performed over the last two decades, and most researches have focused on factors influencing the fatigue life of Zr-4 components, like temperature, irradiation, heat treatment conditions and hydrogenation [1,5–8]. However, attention has not been paid to the ratcheting behavior of the material. Ratcheting can deteriorate the performances of a component by permanent strain accumulation damage in a particular direction [9,10]. This may lead to cyclic damage by continuous thinning of the component cross-section. In other words, the accumulation of ratcheting strain due to cyclic plastic deformation in these components can accelerate the fatigue failure. It has been reported that the failure mode of piping components under seismic loading is fatigue with ratcheting and the reduction of fatigue life is attributed to the accumulated ratcheting strain [11,12]. Hence, it is significant to model the material's ratcheting behavior which can provide some theoretical basis for engineering design.

The ratcheting behavior of some other materials has been experimentally investigated [10,13–27]. Simultaneously, some constitutive models have been developed to simulate the ratcheting behavior of materials. A class of models tries to capture the ratcheting behavior by describing the evolution of the yield surface in the deviatoric stress space using kinematic hardening rules [28–32]. The well-known Armstrong and Frederick kinematic hardening rule (A–F rule), based on strain hardening and dynamic recovery of back stress [33], has been reported to overestimate ratcheting strain [29,31,32,34,35]. Models with modification of the dynamic recovery term in the A–F kinematic hardening rule have been proposed to improve the predicting ability [13,22,31,32,35–41]. To predict the anisotropic behavior of the materials, some models have already been proposed [42–49]. Among these, the non-linear kinematic hardening rule with the critical state for dynamic recovery developed by Ohno and Wang [31,32]. The introduction of a critical state and a power function for each dynamic recovery term enables the Ohno–Wang model to yield good prediction of uniaxial ratcheting. However, the anisotropic uniaxial ratcheting behavior cannot be predicted by this model.

A series of monotonic tensile, compressive and uniaxial ratcheting tests were conducted at room temperature in this study. The tests will be the underpinning for later work where reactor conditions of high temperatures and irradiation will apply. The experimental results show that the material features anisotropy both in monotonic tests and uniaxial ratcheting tests at room temperature.

* Corresponding author. Tel.: +86 22 27408399; fax: +86 22 27403389.
*E-mail address:* xchen@tju.edu.cn (X. Chen).

0022-3115/$ - see front matter © 2013 Elsevier B.V. All rights reserved.
http://dx.doi.org/10.1016/j.jnucmat.2013.06.052

**Table 1**
Chemical compositions of Zr-4 (wt.%).

| Zr | Sn | Fe | Cr | Nb | Cu | Ti | Hf | O | N | H |
|---|---|---|---|---|---|---|---|---|---|---|
| Bal. | 1.5 | 0.2 | 0.1 | <0.01 | <0.002 | <0.0014 | <0.01 | 0.09 | 0.003 | 0.001 |

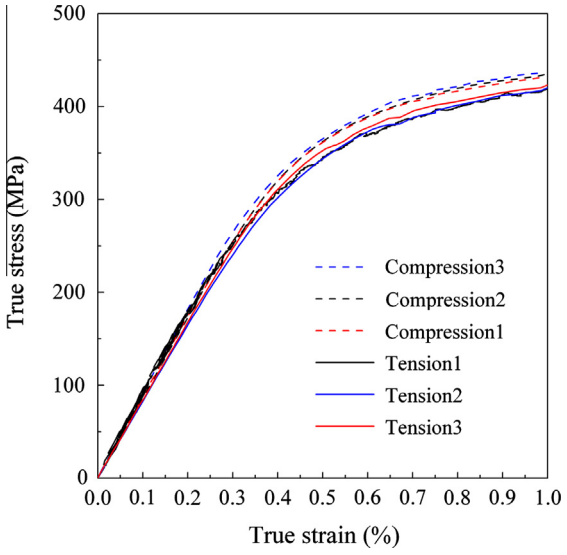


**Fig. 1.** The true stress–strain curves of monotonic tension and compression.

An anisotropic Ohno–Wang (OW) constitutive model introducing an initial back stress was developed to describe the anisotropic uniaxial ratcheting behavior of Zr-4 with different mean stress directions at room temperature. The results predicted by the anisotropic OW model proved to be more reasonable than those by the isotropic OW model for uniaxial ratcheting with different mean stress directions.

## 2. Experimental

The chemical compositions of Zr-4 alloy used in this study are given in Table 1. All test specimens were tubular, with a test section of 9.5 mm outside diameter, 0.6 mm wall thickness and 100 mm length. All the specimens were tested as received. The as-received specimens had been subjected a recrystallized heat treatment of 2 h at 540 °C in a vacuum, resulting in an equiaxial grain size of approximately 5 μm. Tests were conducted on a 20-kN closed-loop servo-hydraulic tension–compression testing machine with a digital controller using an extensometer with a gauge length of 12.5 mm to measure the axial deformation.

### 2.1. Monotonic tensile and compressive tests

In this study, the monotonic tensile and compressive tests were first performed at room temperature with the constant strain rate of $10^{-3}$/s. To ensure the reliability of the results, both of the monotonic tests were repeated three times. The results are plotted in true stress versus true strain in Fig. 1, and the results of the compressive tests are presented in absolute values for the easiness of comparison. The fundamental mechanical properties obtained from these tests are listed in Table 2. It can be seen that the 0.2% offset yield stresses obtained by compressive tests are higher than those by tensile tests, respectively. So, it may be concluded that the material exhibits anisotropy in tensile and compressive directions. The mechanical anisotropy of Zr-4 can be attributed to its microstructure especially preferred orientations or textures developed during the fabrication processes involving various thermo-mechanical treatments [47]. The texture of the fabricated material will have a significant effect on its performance because properties such as the yield strength, thermal and in-reactor creep strengths,

**Table 2**
Mechanical properties of Zr-4.

| Loading direction | Young's modulus (GPa) | 0.2% offset yield stress (MPa) | Ultimate tensile stress (MPa) | Total elongation (%) |
|---|---|---|---|---|
| Tensile1 | 85.4 | 367 | 512 | 37.3 |
| Tensile2 | 83.2 | 362 | 506 | 35.1 |
| Tensile3 | 86.2 | 371 | 523 | 35.3 |
| Compressive1 | 88.6 | 387 | – | – |
| Compressive2 | 88.9 | 393 | – | – |
| Compressive3 | 89.1 | 399 | – | – |

**Table 3**
Loading conditions of uniaxial ratcheting tests.

| Specimens No. | Loading step | Stress amplitude (MPa) | Mean stress (MPa) | Number of cycles |
|---|---|---|---|---|
| SP1 | | 180 | 180 | 1000 |
| | Step 1 | 205 | | 1000 |
| SP2 | Step 2 | 230 | 180 | 1000 |
| | Step 3 | 205 | | 1000 |
| SP3 | | 230 | 180 | 1000 |
| SP4 | Step 1 | 230 | 155 | 1000 |
| | Step 2 | | 180 | 1000 |
| | Step 3 | | 155 | 1000 |
| SP5 | | 230 | 205 | 1000 |
| SP6 | Step 1 | 230 | −180 | 300 |
| | Step 2 | | 180 | 1000 |
| SP7 | Step 1 | 230 | −180 | 2400 |
| | Step 2 | | 180 | 1000 |

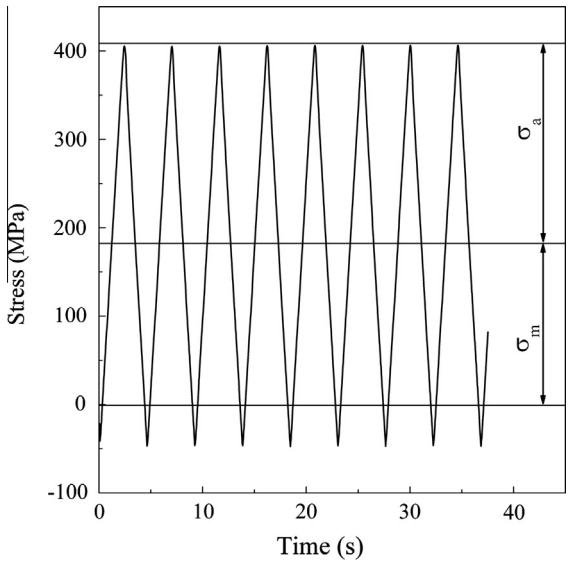


**Fig. 2.** The schematic profile of the loading conditions.

fatigue and stress corrosion cracking resistance, hydride orientation and irradiation induced growth behavior are strong functions of texture [50,51]. Therefore, it is presumably believed that the mechanical anisotropy of Zr-4 observed in this study is attributed to its microstructure especially the texture. Both slip and twinning mechanisms make significant contribution to the development of crystallographic textures. In zirconium alloys, the primary slip system has been found to be the prism slip on $\{10\bar{1}0\}$ planes along $\langle 1\bar{2}10\rangle$ directions [52]. While slip is rarely observed on the basal ($\{0002\}$) planes, cold working seems to harden the prismatic planes thereby making the deformation possible on secondary slip systems such as the basal ($\{0002\}\langle 1\bar{2}10\rangle$) [53]. In recrystallized material tested in our study, the dominant mechanism is the prism slip. The operable twinning modes in zirconium alloys are dependent on the type of loading, and different modes are activated under tension versus compression. Under a tensile stress along the *c*-axis, ($\{10\bar{1}2\}\langle\bar{1}011\rangle$) twins are activated, and less commonly ($\{11\bar{2}1\}\langle\bar{1}\bar{1}26\rangle$) twins operate whereas ($\{11\bar{2}2\}\langle\bar{1}\bar{1}23\rangle$) twins are dominant during compressive loading [47,51].

### 2.2. Uniaxial ratcheting tests

A series of uniaxial ratcheting tests were performed at room temperature in triangular waveform stress-control mode. All tests were conducted with a stress rate of 200 MPa/s, but different mean stresses and stress amplitudes. The loading conditions are shown in Table 3 and a schematic profile of the loading conditions is shown in Fig. 2. A typical stress–strain curve of uniaxial ratcheting and the corresponding ratcheting strain versus cyclic number are plotted in Fig. 3. Here in this study, the ratcheting strain $\varepsilon_r$ is defined as:

$$\varepsilon_r = \frac{\varepsilon_{\max} + \varepsilon_{\min}}{2} \tag{1}$$

where $\varepsilon_{\max}$ and $\varepsilon_{\min}$ are the maximum and minimum axial strain in each cycle, respectively. The ratcheting strain rate $\dot{\varepsilon}_r$ is defined as:

$$\dot{\varepsilon}_r = \frac{d\varepsilon_r}{dN} \tag{2}$$

where $N$ is the number of cycles. It is shown that the ratcheting strain accumulates in the direction of the mean stress. The ratcheting strain rate, which is much higher for the initial 20 cycles, decreases continuously with the increasing cyclic number and almost keeps constant after 100 cycles. More detailed experimental results will be discussed in Section 4.

## 3. Constitutive models

The cyclic plasticity constitutive models employed for ratcheting analysis with the assumption of rate-independent material behavior consist the following three parts:

i. von Mises yield criterion:

$$f = \frac{3}{2}(\boldsymbol{s} - \boldsymbol{\alpha}) : (\boldsymbol{s} - \boldsymbol{\alpha}) - \sigma_0^2 = 0 \tag{3}$$

ii. The plastic flow rule:

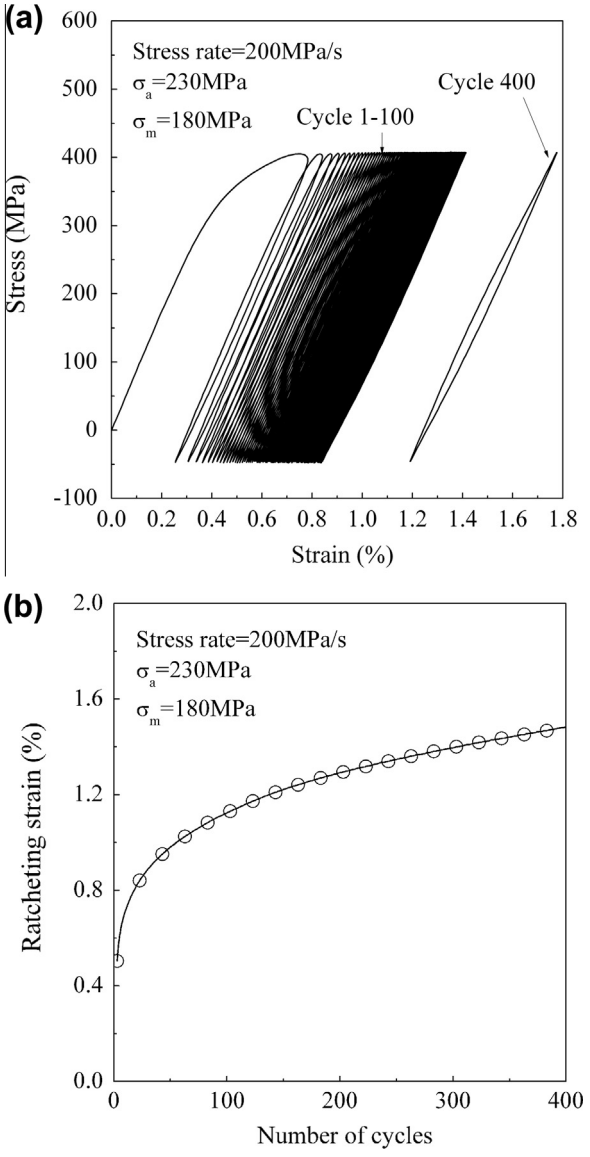


**Fig. 3.** Uniaxial ratcheting test with the stress amplitude of 230 MPa and the mean stress of 180 MPa at stress rate of 200 MPa/s: (a) stress–strain curve and (b) ratcheting strain versus cyclic number.

**Table 4**
The OW model parameters for Zr-4 at room temperature.

| $\sigma_0$ (MPa) | $E$ (GPa) | $v$ | $m_i (i = 1–8)$ |
|---|---|---|---|
| 145 | 86 | 0.3 | 15 |
| $\gamma_{1-8}$ = 5000, 3000, 1000, 200, 100, 50, 20, 14 | | $r_{1-8}$ = 57, 53, 50, 31, 14, 36, 38, 30 MPa | |

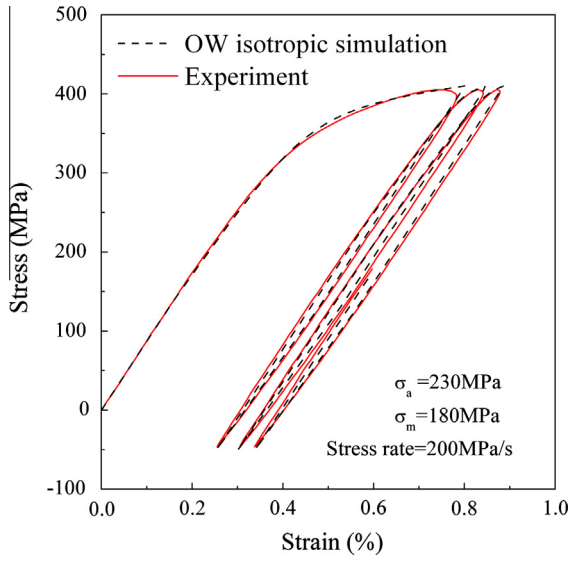


**Fig. 4.** The simulated and experimental stress–strain response of the first three cycles for uniaxial ratcheting tests with tensile mean stress.

$$d\boldsymbol{\varepsilon}^p = \frac{1}{H}\left\langle \frac{\partial f}{\partial \boldsymbol{\sigma}} : d\boldsymbol{\sigma} \right\rangle \frac{\partial f}{\partial \boldsymbol{\sigma}} \tag{4}$$

iii. The kinematic hardening rule :

$$d\boldsymbol{\alpha} = g(\boldsymbol{\sigma}, \boldsymbol{\varepsilon}^p, \boldsymbol{\alpha} d\boldsymbol{\sigma}, d\boldsymbol{\varepsilon}^p, \text{etc.}) \tag{5}$$

where $\boldsymbol{\sigma}$ is the stress tensor, $\boldsymbol{\alpha}$ is the back stress, $\boldsymbol{s}$ is the deviatoric stress tensor, $\sigma_0$ is the initial size of the yield surface, $\boldsymbol{\varepsilon}^p$ is the plastic strain tensor, $H$ is the plastic modulus calculated by using the consistency condition along with three constitutive rules given by Eqs. (3)–(5), and $\langle\rangle$ is the Macauley bracket.

### 3.1. The Ohno–Wang model

The most important feature of ratcheting simulation in cyclic plasticity constitutive models is the kinematic hardening rule that dictates the evolution of the yield surface during a plastic loading increment by translation in the stress space [13,34]. The nonlinear kinematic hardening rule employed in this study is the Ohno–Wang (OW) model [31,32], which is a superposition of several A–F kinematic hardening rules, and assumes that each component of back stress has a critical state for its dynamic recovery term with a slight nonlinearity for each rule. The formula (the OW II model) is proposed as follows:

$$d\boldsymbol{\alpha} = \sum_{i=1}^{M} d\boldsymbol{\alpha}_i, \; d\boldsymbol{\alpha}_i = \gamma_i \left[ \frac{2}{3} r_i d\boldsymbol{\varepsilon}^p - \left( \frac{\bar{\boldsymbol{\alpha}}_i}{r_i} \right)^{m_i} \left\langle d\boldsymbol{\varepsilon}^p : \frac{\boldsymbol{\alpha}_i}{\bar{\boldsymbol{\alpha}}_i} \right\rangle \boldsymbol{\alpha}_i \right], f_i = \bar{\boldsymbol{\alpha}}_i^2 - r_i^2, \tag{6}$$

where $\boldsymbol{\alpha}_i$ is the $i$th component of deviatoric back stress, $\bar{\boldsymbol{\alpha}}_i$ is the magnitude of $\boldsymbol{\alpha}_i$, $\bar{\boldsymbol{\alpha}}_i = \sqrt{3/2(\boldsymbol{\alpha}_i : \boldsymbol{\alpha}_i)}$, and $\gamma_i$, $r_i$ are material parameters. $f_i$ indicates the critical state of dynamic recovery. In this model, before reaching its critical state the dynamic recovery term is partially operative, hence producing incompletely closed stress-controlled hysteresis loops and allowing uniaxial ratcheting to occur. $m_i$ is a material constant, and with the smaller value of $m_i$, the model predicts the higher ratcheting strain. When $m_i \to +\infty$, the modified model is reduced to a former model (the OW I model, not shown here) also proposed by Ohno and Wang, which predicts no uniaxial ratcheting [34].

A large number of decomposed rules should be employed in the OW model in order to simulate the nonlinear hysteresis curve. All the parameters in the OW model can be determined from uniaxial tests, and the parameter determination scheme has already been discussed in detail [34]. In this study, it is found that eight terms of hardening rule are sufficient to obtain a good stable uniaxial hysteresis loop simulation for Zr-4. The values of the material parameters $\gamma_i$ and $r_i$ are determined from monotonic tensile curve. The material parameters $m_i$ for each component $\boldsymbol{\alpha}_i$ are assumed to be the same for convenience and can be determined by trial to simulate a uniaxial ratcheting test. All the material parameters of the OW model for Zr-4 are presented in Table 4.

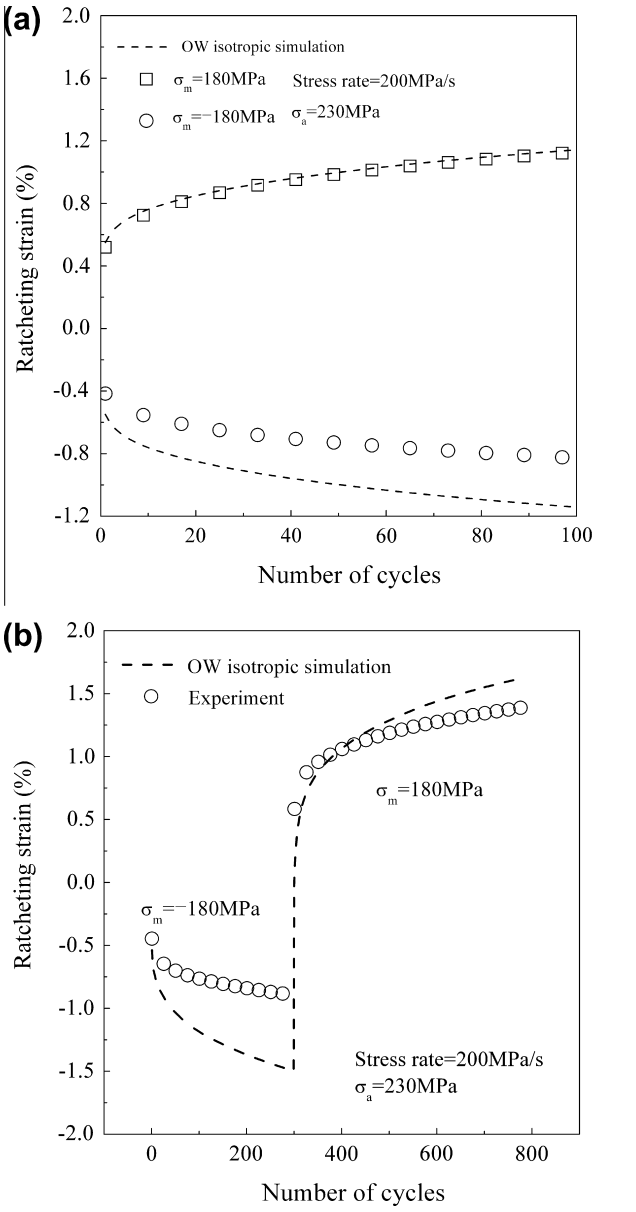


**Fig. 5.** Ratcheting strain evolution: (a) with different mean stress directions and (b) with loading history of cycling under compressive mean stress.

Fig. 4 shows typical stress–strain response of the first three cycles for the test with tensile mean stress simulated by the OW model with those material parameters presented in Table 4. It can be seen that the OW model can simulate the ratcheting behavior well for the case under tensile mean stress.

Fig. 5a plots the ratcheting strain evolution of the tests under the same loading conditions but the tensile and compressive mean stress, and their corresponding simulation results predicted by the OW model. It is noticed that the simulation result of the test under

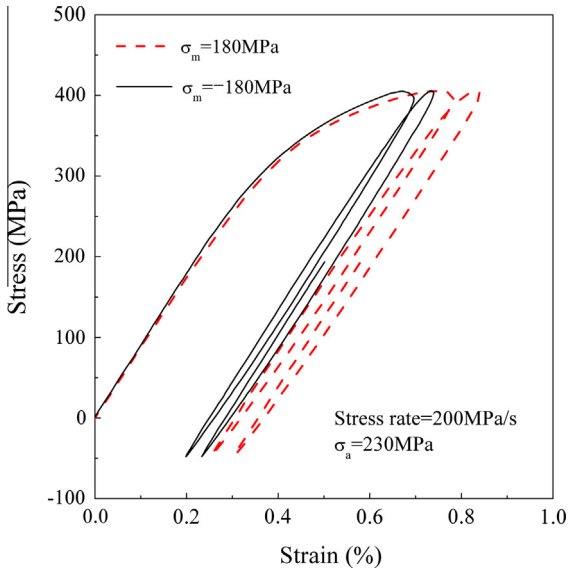


**Fig. 6.** Stress–strain response of the first two cycles for uniaxial ratcheting tests with different mean stress directions.

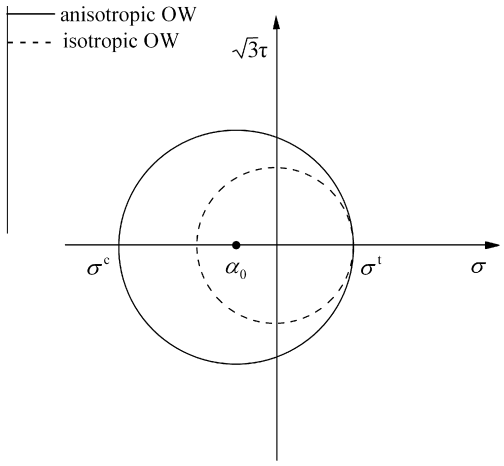


**Fig. 7.** The initial yield surface after introduced an initial back stress.

compressive mean stress deviates from the corresponding experimental result to an unacceptable degree. Actually, the simulation results of the tests under different mean stress directions are the same except for the sign. This is because the material parameters adopted in the OW model are the same but the sign of mean stress. As seen, the OW model with the material parameters determined from the monotonic tensile curve cannot predict the ratcheting behavior of the tests with compressive mean stress well, and vice versa.

The predicted ratcheting strain evolution of tests with history of cycling under compressive mean stress is presented in Fig. 5b. It is seen that the simulation result deviates from the experimental result in the first step with compressive mean stress, which can be attributed to the same reason mentioned above. Furthermore, the simulation result in the second step is not good, although the OW model can simulate the ratcheting behavior of test with tensile mean stress without loading history well. The poor prediction for the first step under compressive mean stress is believed to deteriorate the simulation of the subsequent step under tensile mean stress.

### 3.2. An anisotropic model

From the comparison of experimental and simulation results shown in Fig. 5, one can see that the OW model cannot predict the tests with compressive mean stress well. It is presumably believed that the mechanical anisotropy of Zr-4 contributes to the deviation of the simulation results from the experimental results of the tests with compressive mean stress. Fig. 6 shows the stress–strain response of the first two cycles for uniaxial ratcheting tests with different mean stress directions (tensile and compressive). In order to compare the ratcheting strains between tests with tensile mean stress and compressive stress, the compressive direction is regarded as the positive direction for tests with compressive mean stress. It can be observed that their initial yield stresses in the first cycles are discrepant, which is consistent with the results from monotonic tests. It can also be seen that stress of the specimen under compressive mean stress reaches the peak value at a smaller strain due to its higher yield stress. The same goes for each of the following cycles. Therefore, the ratcheting strain of the specimen under compressive mean stress is smaller for each cycle. As a result, the overall ratcheting strain level of the specimen under compressive mean stress is smaller than that under tensile mean stress. So, it can be concluded that the difference of the yield stress greatly influences the ratcheting behavior, even though the other loading conditions are the same. Therefore, to predict the anisotropic behavior of the material, attention should be paid to the yield stress.

An initial back stress tensor is introduced to the von Mises yield surface to describe the anisotropy of Zr-4. The initial back stress is used to adjust the center offset of the yield surface such that the initial yield stress will match the experimental values. Thus, the applicability of the OW model can be improved to anisotropic materials.For the cases of uniaxial ratcheting responses in this study, the initial back stress $\alpha_0$ is defined as:

$$\alpha_0 = \frac{\sigma^t - \sigma^c}{2} \tag{7}$$

where $\sigma^t$ and $\sigma^c$ are the initial tensile yield stress and compressive yield stress of the material, respectively. Here, the initial size of the yield surface $\sigma_0$ is defined as:

$$\sigma_0 = \sigma_0^t - \alpha_0 \tag{8}$$

The initial yield surface after translation is plotted in Fig. 7 for anisotropic OW model as solid line, but the yield surface of OW model is dash line.

The plastic flow rule and the nonlinear kinematic hardening rule employed in the model are still the ones in OW model. $\sigma^t$ and $\sigma^c$ can be obtained from the monotonic uniaxial tensile test and compressive test, respectively, and then the initial back stress $\alpha_0$ and the initial size of the yield surface $\sigma_0$ can be determined. All

**Table 5**
The anisotropic OW model parameters for Zr-4 at room temperature.

| $\sigma^t$ (MPa) | $\sigma^c$ (MPa) | $\alpha_0$ (MPa) | $\sigma_0^t$ (MPa) | $\sigma_0$ (MPa) | $E$ (GPa) | $\nu$ | $m_i$ ($i$ = 1–8) |
|---|---|---|---|---|---|---|---|
| 367 | 387 | −10 | 145 | 155 | 86 | 0.3 | 15 |
| $\gamma_{1-8}$ = 5000, 3000, 1000, 200, 100, 50, 20, 14 | | | | $r_{1-8}$ = 57, 53, 50, 31, 14, 36, 38, 30 MPa | | | |

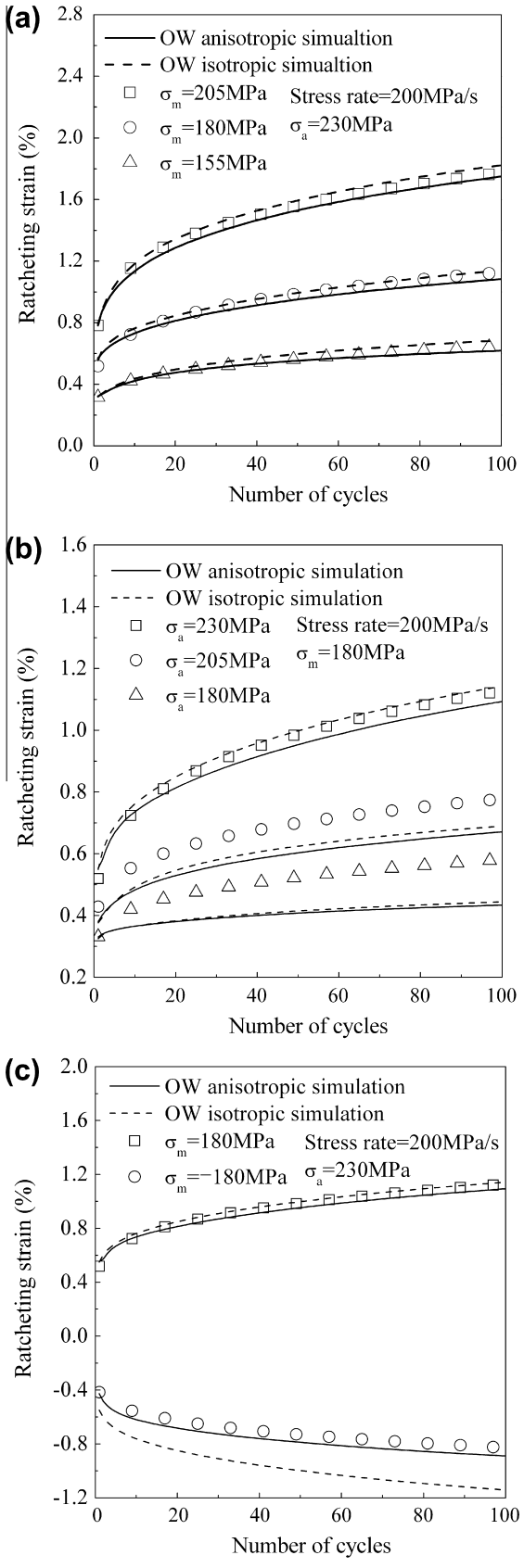


**Fig. 8.** Ratcheting strain evolution with cyclic number under various loading conditions: (a) with different mean stresses, (b) with different stress amplitudes and (c) with different mean stress directions.

other parameters in the model are determined from uniaxial tests, and are the same as that of the OW model (Table 4). For Zr-4 used in this study, the parameters of the OW model with initial anisotropic yield surface are presented in Table 5.

## 4. Simulation results

Comparisons of experimental and simulation results of ratcheting strain evolution for uniaxial ratcheting tests under various loading conditions are presented in Fig. 8. Experimental results in Fig. 8a and b shows that higher stress amplitude or mean stress leads to higher ratcheting strain level. It seems that the ratcheting strain rate almost keeps constant after initial several cycles, and the constant ratcheting strain rate increases with the ratcheting strain level. Fig. 8c shows that the ratcheting strain level of the test under tensile mean stress is higher than that under compressive mean stress even though the magnitude of mean stress and other loading conditions are the same.

From the simulated results shown in Fig. 8a and b, it can be seen that the isotropic OW model produces reasonable predictions for most tests with a relatively higher ratcheting strain level. However, a few uniaxial tensile ratcheting responses cannot be simulated well as shown in Fig. 8b. This is because the material parameter $m_i$ in the model, which controls the ratcheting strain rate, is determined from only one uniaxial ratcheting test (high stress level $\sigma_a$ = 230 MPa, $\sigma_m$ = 180 MPa) and then applied to all other cases as a fixed value [18]. It can also be seen that there is little difference between the simulation results produced by the anisotropic OW model and those by the isotropic OW model. Fig. 8c shows that the simulation results produced by the isotropic OW model for the test under compressive mean stress deviate from the corresponding experimental result to an unacceptable degree. But the ratcheting strain predicted by the anisotropic OW model proves to be in much better agreement with the experimental result under compressive mean stress.

Comparisons of experimental and simulation results of multistep uniaxial ratcheting tests are presented in Fig. 9. As seen from Fig. 9a and b, the ratcheting strain of subsequent cycling under higher stress level continues to accumulate in spite of the prior cycling under lower stress level. However, the ratcheting strain nearly stops to accumulate due to the previous cycling under higher stress level. This can be explained by the work-hardening caused by the prior cycling with high stress level. The hardening effect of material under previous cyclic loading with lower stress level is not significant and can be ignored [54]. It can also be found from Fig. 9a and b that the predicted ratcheting strain level by the anisotropic OW model is lower than that by the isotropic OW model, which can also be found in Fig. 8a and b.

The predicted ratcheting strain evolution of tests with loading history of cycling under compressive mean stress obtained by the isotropic OW model deviates greatly from the experimental results as shown in Fig. 9c and d. On the contrary, the predicted results by the anisotropic OW model show reasonable agreement with the experimental data. It demonstrates that the introduced initial back stress enables the model to predict the uniaxial ratcheting behavior of tests with different mean stress directions.

## 5. Discussion

From Figs. 8 and 9, it can be observed that the simulation results produced by the anisotropic OW model do not coincide with those of the isotropic OW model for uniaxial ratcheting tests with tensile mean stress. Take the case with the stress amplitude of 230 MPa and the mean stress of 180 MPa shown in Fig. 10a for example. The ratcheting strain of the first cycle predicted by the anisotropic OW model is a little higher than that by the isotropic OW model, but the rate is in reverse. After the second cycle, the ratcheting

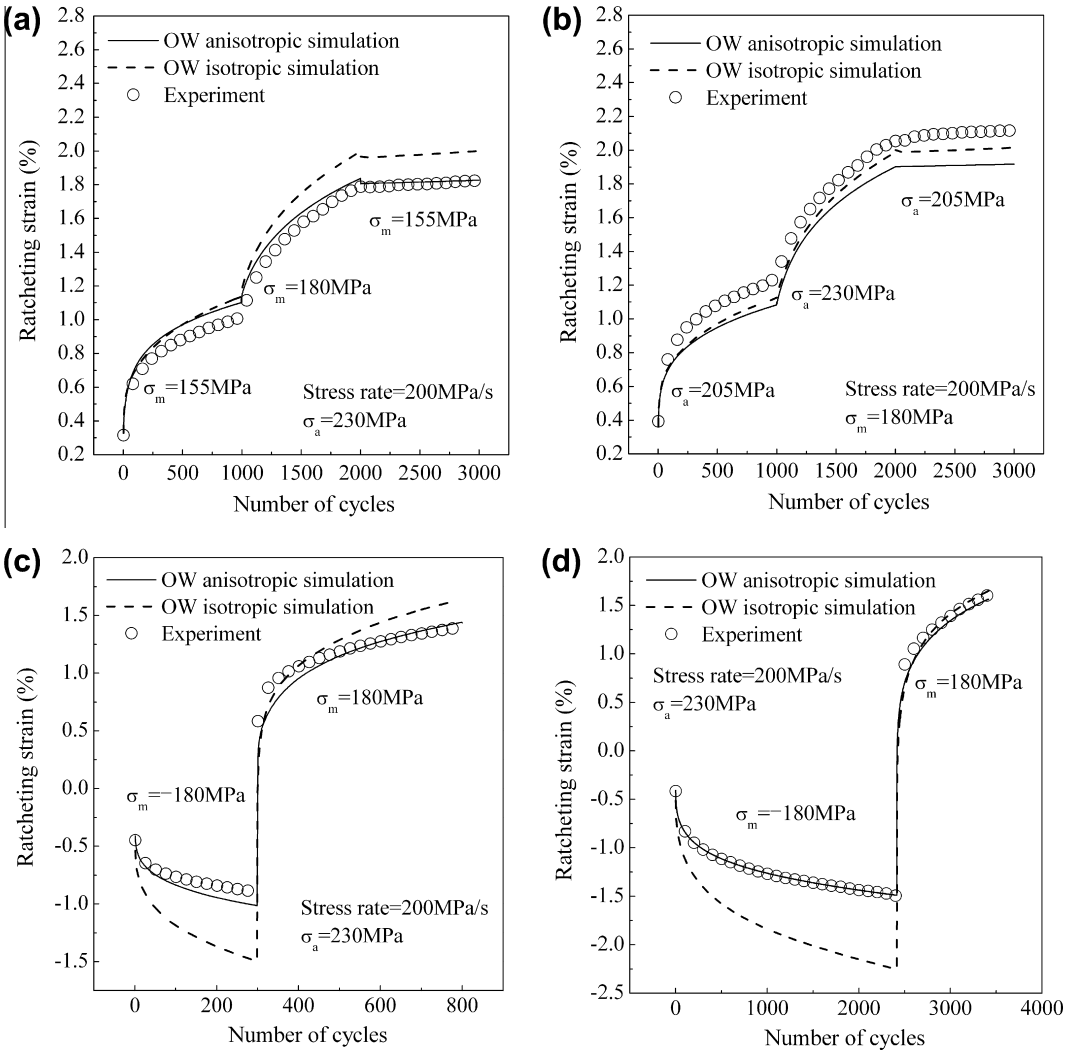


**Fig. 9.** Ratcheting strain evolution of multistep uniaxial ratcheting test under various loading conditions: (a) with various mean stresses, (b) with various stress amplitudes, (c) and (d) with various mean stress directions.

strain predicted by the anisotropic OW model is lower than that by the isotropic OW model with increase in number of cycles as shown in Fig.8. The two curves predicted by isotropic and anisotropic model cross at second cycle.

This phenomenon can be attributed to the different size of the yield surfaces in the two models. The size of the yield surface (145 MPa) in the isotropic OW model is determined from the tensile test because the material is considered initially isotropic as shown in Fig.7 (dash line). While, the experimental results show that Zr-4 is initially anisotropic and the compressive yield stress is higher than the tensile one. So, the size of the yield surface in the anisotropic OW model is determined by both the tensile and compressive yield stress, and the average yield stress should be larger than that in the isotropic OW model. Here, the introduced initial back stress is used to translate the center of the normalized yield surface but to enlarge the initial size of the yield surface (155 MPa) such that the initial yield stress will match the experimental value as shown in Fig. 7 (solid line). Thus, although the initial tensile yield stress is the same, the stress predicted by isotropic OW model reaches the compressive yield stress first due to the smaller value of the yield stress and therefore it reaches the prescribed valley stress at a smaller strain. As a result, the ratcheting strain of the first cycle predicted by the anisotropic OW model is a little higher than that by the isotropic OW model as shown in Fig. 10b. For the second cycles, the ratcheting strain of each cycle predicted by the anisotropic OW model is smaller due to the larger size of the yield surface as shown in Fig. 10c. That is, the ratcheting strain predicted by the anisotropic OW model accumulates slower. Therefore, the ratcheting strain of the first cycle is a little higher but for following cycles, the ratcheting strain predicted by the anisotropic OW model is smaller than that by the isotropic OW model because the the yield surface size is larger for anisotropic OW model, which sheds light on the cross of the two predicted curves.

## 6. Conclusions

From the above mentioned experimental investigation and constitutive modeling for the uniaxial ratcheting behavior of Zr-4 alloy, the following conclusions can be drawn:

(1) The material displays anisotropic behavior both in monotonic tests and uniaxial ratcheting tests with different mean stress directions at room temperature.
(2) The difference of mechanical properties under tensile and compressive loading, especially the yield stress, is believed to contribute to anisotropic ratcheting behavior of the material.

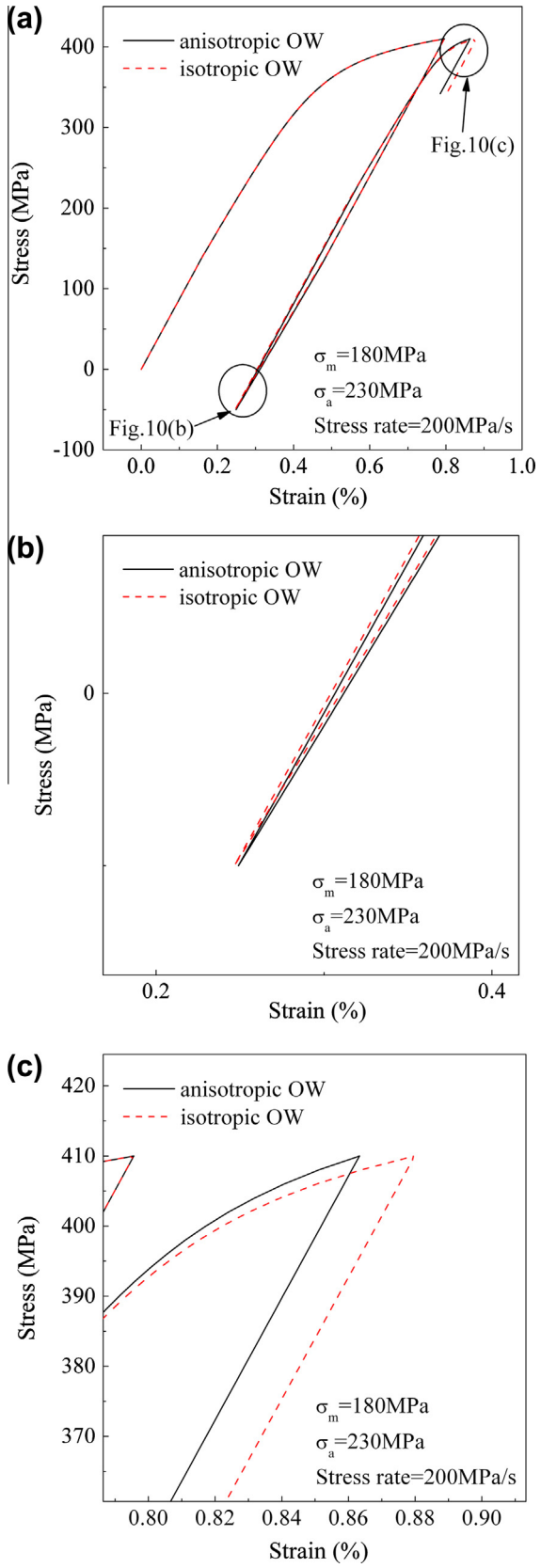


**Fig. 10.** Comparsion of OW model and anisotropic OW model: (a) stress–strain hysteresis loop, (b) unloading point of first cycle and (c) maximum stress point of second cycle.

(3) An anisotropic OW model introduced an initial back stress to the yield surface is developed to describe the anisotropic uniaxial ratcheting behavior of Zr-4 under various loading conditions at room temperature.
(4) The simulation results produced by the anisotropic OW model show much better agreement with the experiments under compressive mean stress. There is little difference between the simulation results produced by the anisotropic OW model and those of the isotropic OW model for the tests under tensile mean stress.
(5) The ratcheting strain of the first cycle is a little higher but for the following cycles, the ratcheting strain predicted by the anisotropic OW model is smaller than that by the isotropic OW model because the yield surface size is larger for anisotropic OW model.

## Acknowledgements

The authors gratefully acknowledge financial support for this work from the National High Technology Research and Development Program of China (863 Program 2009AA04Z403) and Ph.D. Programs Foundation of Ministry of Education of China (No. 20090032110016).

## References

[1] V. Mallipudi, S. Valance, J. Bertsch, Mech. Mater. 51 (2012) 15–28.
[2] L. Xiao, H. Gu, J. Nucl. Mater. 265 (1999) 213–217.
[3] L. Xiao, Y. Umakoshi, J. Sun, Mater. Sci. Eng. A 292 (2000) 40–48.
[4] L. Xiao, H. Gu, Mater. Sci. Eng. A 252 (1998) 166–173.
[5] I. Alvarez-Armas, S. Hereñú, J. Nucl. Mater. 334 (2004) 180–188.
[6] M. Le Saux, J. Besson, S. Carassou, C. Poussard, X. Averty, Eng. Fail. Anal. 17 (2010) 683–700.
[7] J.H. Huang, S.P. Huang, J. Nucl. Mater. 208 (1994) 166–179.
[8] M.K. Samal, G. Sanyal, J.K. Chakravartty, Eng. Fail. Anal. 18 (2011) 2042–2053.
[9] S.K. Paul, S. Sivaprasad, S. Dhar, S. Tarafder, Mech. Mater. 43 (2011) 705–720.
[10] S.K. Paul, S. Sivaprasad, S. Dhar, S. Tarafder, J. Nucl. Mater. 401 (2010) 17–24.
[11] T. Fujiwaka, R. Endou, F. Shin-ichi, S. Ono, K. Oketani, ASME PVP 387 (1999) 19–26.
[12] V. Matzen, Y. Zhu, T. Hassan, Trans. SMIRT 13 (1995) 471–476.
[13] X. Chen, R. Jiao, K.S. Kim, Int. J. Plasticity 21 (2005) 161–184.
[14] N. Bai, X. Chen, Int. J. Plasticity 25 (2009) 2181–2203.
[15] G. Chen, X. Chen, Int. J. Solids Struct. 43 (2006) 3596–3612.
[16] G. Chen, S.-C. Shan, X. Chen, H. Yuan, Comp. Mater. Sci. 46 (2009) 572–578.
[17] X. Chen, D.-H. Yu, K.S. Kim, Mater. Sci. Eng. A 406 (2005) 86–94.
[18] D. Yu, G. Chen, W. Yu, D. Li, X. Chen, Int. J. Plasticity 28 (2012) 88–101.
[19] B. Gao, X. Chen, G. Chen, Int. J. Pres. Ves. Pip. 83 (2006) 96–106.
[20] C. Li, G. Chen, X. Chen, W. Zhang, Comp. Mater. Sci. 57 (2012) 43–47.
[21] G. Kang, Q. Gao, X. Yang, Int. J. Nonlinear Mech. 39 (2004) 843–857.
[22] G. Kang, Q. Gao, X. Yang, Mech. Mater. 34 (2002) 521–531.
[23] T. Hassan, L. Taleb, S. Krishna, Int. J. Plasticity 24 (2008) 1863–1889.
[24] E. Corona, T. Hassan, S. Kyriakides, Int. J. Plasticity 12 (1996) 117–145.
[25] S.M. Rahman, T. Hassan, E. Corona, Int. J. Plasticity 24 (2008) 1756–1791.
[26] Y. Jiang, H. Sehitoglu, Int. J. Plasticity 10 (1994) 579–608.
[27] Y. Jiang, H. Sehitoglu, Int. J. Plasticity 10 (1994) 849–870.
[28] M. Abdel-Karim, Int. J. Plasticity 26 (2010) 711–730.
[29] M. Abdel-Karim, Int. J. Plasticity 25 (2009) 1560–1587.
[30] G. Kang, Mech. Mater. 36 (2004) 299–312.
[31] N. Ohno, J.D. Wang, Int. J. Plasticity 9 (1993) 375–390.
[32] N. Ohno, J.D. Wang, Int. J. Plasticity 9 (1993) 391–403.
[33] P.J. Armstrong, C.O. Frederick, CEGB Report, No. RD/B/N 731, 1966.
[34] S. Bari, T. Hassan, Int. J. Plasticity 16 (2000) 381–409.
[35] J.L. Chaboche, Int. J. Plasticity 7 (1991) 661–678.
[36] Y. Jiang, P. Kurath, Int. J. Plasticity 12 (1996) 387–415.
[37] M. Abdel-Karim, Int. J. Pres. Ves. Pip. 87 (2010) 170–176.
[38] M. Abdel-Karim, N. Ohno, Int. J. Plasticity 16 (2000) 225–240.
[39] X. Chen, R. Jiao, Int. J. Plasticity 20 (2004) 871–898.
[40] B. Berisha, P. Hora, A. Wahlen, L. Tong, Int. J. Plasticity 26 (2010) 126–140.
[41] S. Bari, T. Hassan, Int. J. Plasticity 17 (2001) 885–905.
[42] H. Yao, J. Cao, Int. J. Plasticity 18 (2002) 1013–1038.
[43] T. Böhlke, A. Bertram, E. Krempl, Int. J. Plasticity 19 (2003) 1867–1884.
[44] D. Ciurchea, J. Nucl. Mater. 131 (1985) 1–10.
[45] L. Delannay, M.R. Barnett, Int. J. Plasticity 32–33 (2012) 70–84.

[46] P. Delobelle, P. Robinet, P. Geyer, P. Bouffioux, J. Nucl. Mater. 238 (1996) 135–162.
[47] K. Linga Murty, I. Charit, Prog. Nucl. Energy 48 (2006) 325–359.
[48] J. Ning, E.C. Aifantis, Int. J. Plasticity 12 (1996) 1221–1240.
[49] J. Ning, E.C. Aifantis, Int. J. Plasticity 11 (1995) 183–193.
[50] R.G. Ballinger, G.E. Lucas, R.M. Pelloux, J. Nucl. Mater. 126 (1984) 53–69.
[51] E. Tenckhoff, ASTM 966, Philadelphia, PA, USA, 1988.
[52] E. Tenckhoff, J. ASTM Int. 2 (2005) 1.
[53] K.L. Murty, B.L. Adams, ASTM 765, Philadelphia, PA, USA, 1982.
[54] G. Chen, X. Chen, C.-D. Niu, Mater. Sci. Eng. A 421 (2006) 238–244.